Microchimica Acta (2022) 189: 317
https://doi.org/10.1007/s00604-022-05429-9

ORIGINAL PAPER

Electrochemiluminescence biosensor for determination of lead(II) ions using signal amplification by Au@SiO_2 and tripropylamine-endonuclease assisted cycling process

Hongguo Zhai[1,2,3] · Yue Wang[1,2,3] · Jiaqi Yin[1,2,3] · Yuhao Zhang[1,2,3] · Qi Guo[1,2,3] · Xia Sun[1,2,3] · Yemin Guo[1,2,3] · Qingqing Yang[1,2,3] · Falan Li[1,2,3] · Yanyan Zhang[1,2,3]

Received: 2 May 2022 / Accepted: 8 July 2022 / Published online: 5 August 2022

Abstract

MXene@Au as the base and Au@SiO_2 as signal amplification factor were used for constructing an ultrasensitive "on–off" electrochemiluminescence (ECL) biosensor for the detection of Pb^{2+} in water. The use of MXene@Au composite provided a good interface environment for the loading of tris(2,2-bipyridyl)ruthenium(II) ($Ru(bpy)_3^{2+}$) on the electrode. Based on resonance energy transfer, the Au (core) SiO_2 (shell) (Au@SiO_2) nanoparticles stimulate electron transport and promote tripropylamine (TPrA) oxidation. The luminescence effect of Au@SiO_2 was five times that of AuNPs and SiO_2 nanomaterials alone, and the ECL intensity was greatly improved. In addition, Pb^{2+} activated the aptamer to exert its endonuclease activity, which realized the signal cycle amplification in the process of Pb^{2+} detection. When Pb^{2+} was added, the ECL signal weakened, and the Pb^{2+} concentration was detected according to the decreased ECL intensity. Under optimized experimental conditions, this aptamer sensor for Pb^{2+} has a wide detection range (0.1 to 1×10^6 ng L^{-1}) and a low detection limit (0.059 ng L^{-1}). The relative standard deviation (RSD) of the sensor is 0.39–0.99%, and the recovery of spiked standard is between 90.00 and 125.70%. The sensor shows good selectivity and high sensitivity in actual water sample analysis. This signal amplification strategy possibly provides a new method for the detection of other heavy metal ions and small molecules.

Keywords Electrochemiluminescence · Aptamer sensor · MXene@Au · Au@SiO_2

Introduction

With the improvement of people's living standards, human activities have led to the increase of heavy metal content in the environment, resulting in serious water pollution; Pb^{2+} does great harm to the growth of aquatic organisms and the safety of human life [1–4]. Therefore, rapid and sensitive methods for detecting heavy metals are urgently needed. At present, the traditional detection methods for heavy metals mainly include gas chromatography (GC), high-performance liquid chromatography (HPLC), and inductively coupled plasma mass spectrometry (ICP-MS). Although these methods are relatively mature and have the characteristics of high sensitivity, high accuracy, and wide detection range, their wide application is greatly limited by the high cost and time-consuming usage of the instrument [5, 6].

Therefore, it is still urgent to find a simple, rapid, and sensitive detection technology for ions. Among them, electrochemiluminescence (ECL) has achieved great success in detection because of its low background signal, simple operation, and good electrochemical characteristics [7]. However, the detection of trace heavy metals still has the problems of low sensitivity and narrow detection range. In order to further improve the detection sensitivity, the selection of appropriate signal amplification technology has become a research hotspot, for example, reducing graphene oxide [8], quantum dot [9], metal alloy [10], enzyme [11], and other nanomaterials [12, 13]. They can effectively improve the

✉ Yanyan Zhang
zyyan1104@163.com

[1] School of Agricultural Engineering and Food Science, Shandong University of Technology, No. 266 Xincun Xilu, Zibo 255049, China

[2] Shandong Provincial Engineering Research Center of Vegetable Safety and Quality Traceability, No. 266 Xincun Xilu, Zibo 255049, China

[3] Zibo City Key Laboratory of Agricultural Product Safety Traceability, No. 266 Xincun Xilu, Zibo 255049, China

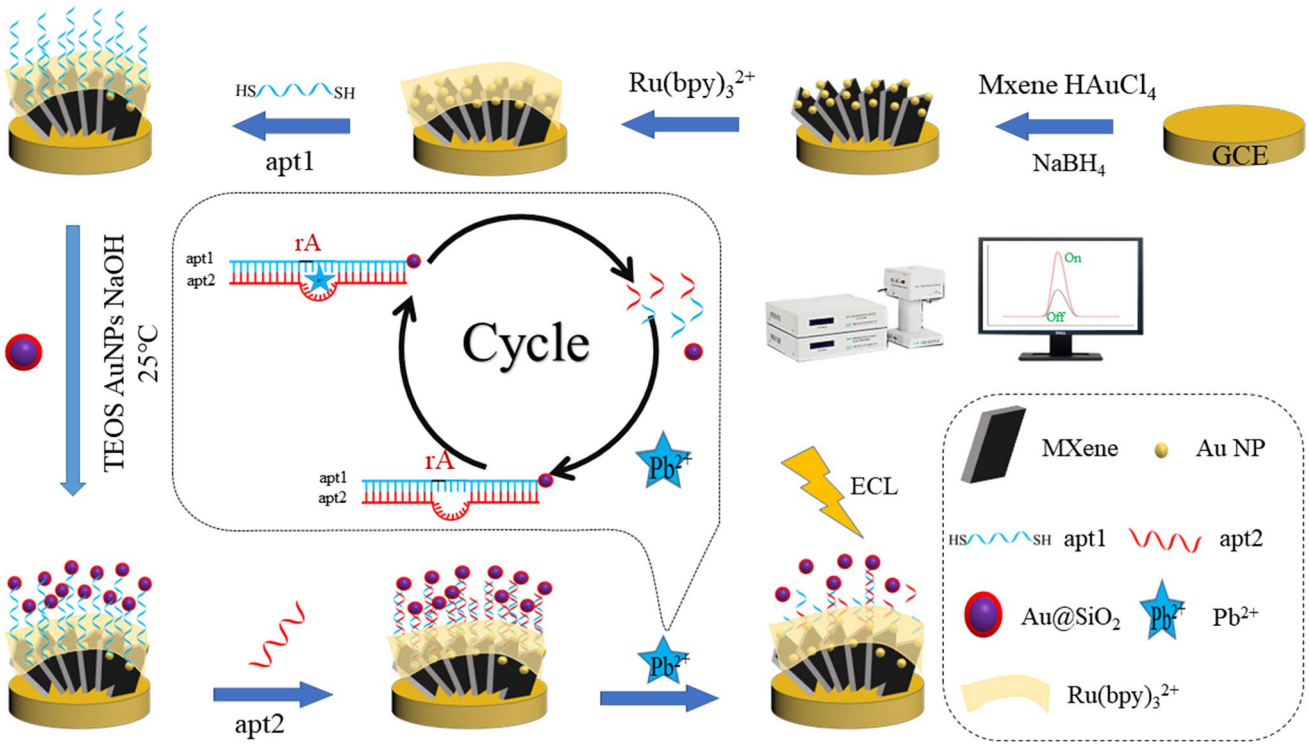

Scheme 1. Schematic diagram of the sensor assembly process

sensor interface environment and catalyze the reaction system by increasing the specific surface area of the electrode surface and improving the electron transfer rate. Therefore, in this paper, two signal amplification techniques of nanomaterials and enzymes were used to improve the sensitivity of the sensor. Although the above experimental design can also achieve the detection of high sensitivity, the volume of metal ions are small and difficult to capture, which has limitations on the development of heavy metal ion detection strategy. Therefore, aptamer is a good specific biometric element.

Aptamer is an oligonucleotide fragment obtained from nucleic acid molecular library, which has not only high sensitivity, strong detection, but also strong specificity [14–16]. On the one hand, the ECL aptamer sensor can use the advantage of ECL. On the other hand, it can combine aptamer specificity to capture ability. At present, it has become a research hotspot in many fields such as molecular biology, clinical diagnosis, medical research, and rapid quarantine [17]. Therefore, using the ECL aptamer sensor to detect heavy metals in environment has a good application prospect.

Therefore, this work used MXene@Au as the base material of the fixed aptamer to improve the conductivity of the sensor. With the help of Au@SiO_2 core–shell nanomaterial and aptamer cascade assisted cycling, an ultra-sensitive "on–off" electrochemiluminescence biosensor for Pb^{2+} detection was constructed. The large specific surface area of MXene@Au had become a good carrier loaded with $Ru(bpy)_3^{2+}$, which could significantly amplify electrochemical sensing signals. It was found that in the electrochemiluminescence system of $Ru(bpy)_3^{2+}$/TPrA, based on resonance energy transfer, the Au@SiO_2 core–shell nanomaterial could improve the excitation rate of $Ru(bpy)_3^{2+}$, accelerating TPrA oxidation. Thus, the electrochemiluminescence intensity was greatly improved. In addition, the aptamer could be used as recognition element and cascaded enzyme assisted circulation, which improved the sensitivity of the sensor. The biosensor construction process was shown in Scheme 1.

Materials and methods

Material

Aptamer and 1 × TE buffer were obtained from Shanghai Shenggong Biotechnology Co., Ltd. Aptamer sequences were synthesized according to previous literature [18]. The mercapto-modified aptamer sequence S1: 5′-(SH)-TGG ATT CGrA GGA AAG AGA TGA TGT CTG T-(SH)-3′, and the complementary aptamer sequence S2: 3′-ACC TAA GCT TGC CGC CGC GAT GAA GTT CTC TAC TAC AGA CA-5′. Trisodium citrate dihydrate, disodium hydrogen citrate ($Na_2HPO_4{\cdot}12H_2O$), sodium dihydrogen citrate

($NaH_2PO_4{\cdot}2H_2O$), sodium borohydride ($NaBH_4$), chitosan (CS), potassium ferricyanide, and tripropylamine were all obtained from Sinopharm Chemical Holdings Co., Ltd. (Shanghai, China). 1% $HAuCl_4{\cdot}3H_2O$, hexahydrate tri(2,2-bipyridine)ruthenium chloride was obtained from Sigma-Aldrich Trading Co., Ltd. (Shanghai, China). Tri (2-carbonyl ethyl)-phosphate hydrochloride (TCEP) was purchased from Beijing Suomobao Technology Co., Ltd. Silicic acid tetraethyl ester (TEOS) was purchased from Tianjin Fuchen Chemical Reagent Factory. Polydiallyl dimethyl ammonium chloride (PDDA) was obtained from Aladdin Reagent (Shanghai) Co., Ltd. Titanium carbide $Ti_3C_2T_x$ (MXene) thin layer dispersion was purchased from Xianfeng Nanomaterials Technology Co., Ltd. (Jiangsu). The experimental water was ultrapure water.

Apparatus

MPI-A electrochemiluminescence workstation (Xi'an Remex Analysis Instruments Co., Ltd., China). CHI660D electrochemical workstation (Shanghai Chenhua Instrument Co., Ltd., China). Three electrode systems were used in the experimental detection, in which platinum wire was used as the auxiliary electrode, Ag/AgCl as the reference electrode, and glassy carbon electrode (GCE, $D = 3$ mm). Varioskan L mycotoxin immunoassay tester. WJGS-032 transmission electron microscope (TEM). LS MK2 PALL-water purification system (18.2 MΩ, 25℃).

Preparation of MXene@Au

MXene@Au was based on the previous literature and had been modified [19–21]. First, 12 mL 0.5 mg mL^{-1} titanium carbide was ultrasonic dispersed for 10 min. Then 60 µL 1% $HAuCl_4{\cdot}3H_2O$ was added and reacted for 30 min. Meanwhile, 50 µL of 0.16 M $NaBH_4$ and 1.6 M sodium hydroxide (NaOH) (volume ratio = 1:1) were added and ultrasonic treated for 30 min. Finally, centrifuged the mixture at 10,000 rpm for 8 min and washed with ultrapure water for three times and vacuum dried at 60℃. The 5 mg mL^{-1} solution was prepared.

Preparation of Au@SiO_2 core–shell nanomaterials

The experimental materials were prepared according to the literature and slightly modified [22]. Added 200 mL ultrapure water to 2 mL 1% $HAuCl_4{\cdot}3H_2O$ and heated in the microwave until the solution boils. After that, 1% trisodium citrate was quickly added and heated for 4 min; the solution turned wine red. After cooling at room temperature, ultrapure water was added at constant volume to 200 mL (0.1 mg mL^{-1}).

The preparation process of AuNPs was in the supplementary material.

Preparation of aptamer sensor

The three-electrode system was used in the experiment, and the glassy carbon electrode was finely polished with aluminum oxide powder (0.3 µm and 0.05 µm). Then, the electrode was cleaned with ultrasonic in ultrapure water and alcohol, respectively, and blow-dried with nitrogen for standby.

The biosensor construction process was shown in Scheme 1. First, 5 µL MXene@Au solution was dropped onto a clean electrode surface and dried it at room temperature. Then, 5 µL $Ru(bpy)_3^{2+}$ chitosan solution was coated on the electrode surface. $Ru(bpy)_3^{2+}$ could be adsorbed to the electrode through π-π conjugated bond, and it could bind to the electrode more closely. Then, 5 µL thiol modified aptamer S1 solution was added dropwise on the electrode surface. After incubating for 50 min, the aptamer and AuNPs were fixed on the electrode surface through gold-sulfur bond. Subsequently, 5 µL Au@SiO_2 solution was added to enhance the ECL strength of the sensor. Finally, 5 µL aptamer S2 and S1 were added for complementary base pairing and incubated for 50 min to fully combine. The luminescence effect was tested by dropping 5 µL Pb^{2+} on the modified electrode to verify the performance of the biosensor.

Pretreatment of real samples

In order to verify the detection effect of aptamer sensor on Pb^{2+} in real water samples, tap water, lake water, and industrial wastewater were selected as the experimental objects, and all water sources came from local sources. First of all, the three water samples were centrifuged at 10,000 rpm for 15 min and the supernatant was taken for standby. Secondly, the supernatant solution was filtered with a 0.22-µm filter membrane. A total of 10 µL of Pb^{2+} standard solution was taken, and three kinds of filtrates were diluted to prepare 10 ng/L, 100 ng/L, and 1000 ng/L of Pb^{2+} solution for laboratory use. Dropped 5 µL the prepared Pb^{2+} solution to the working electrode and measured on the electrochemiluminescence workstation under the high voltage 600 V, 0.4–1.2 V of the photomultiplier tube.

Results and discussion

Characterization of MXene@Au

Figure 1A and 1B show MXene@Au morphology of nanocomposites. AuNPs formed by reduction of $NaBH_4$ and NaOH are evenly distributed on MXene, and their particle size are about 25–30 nm. In addition, EDS measurements are made on MXene@Au. Corresponding element mapping

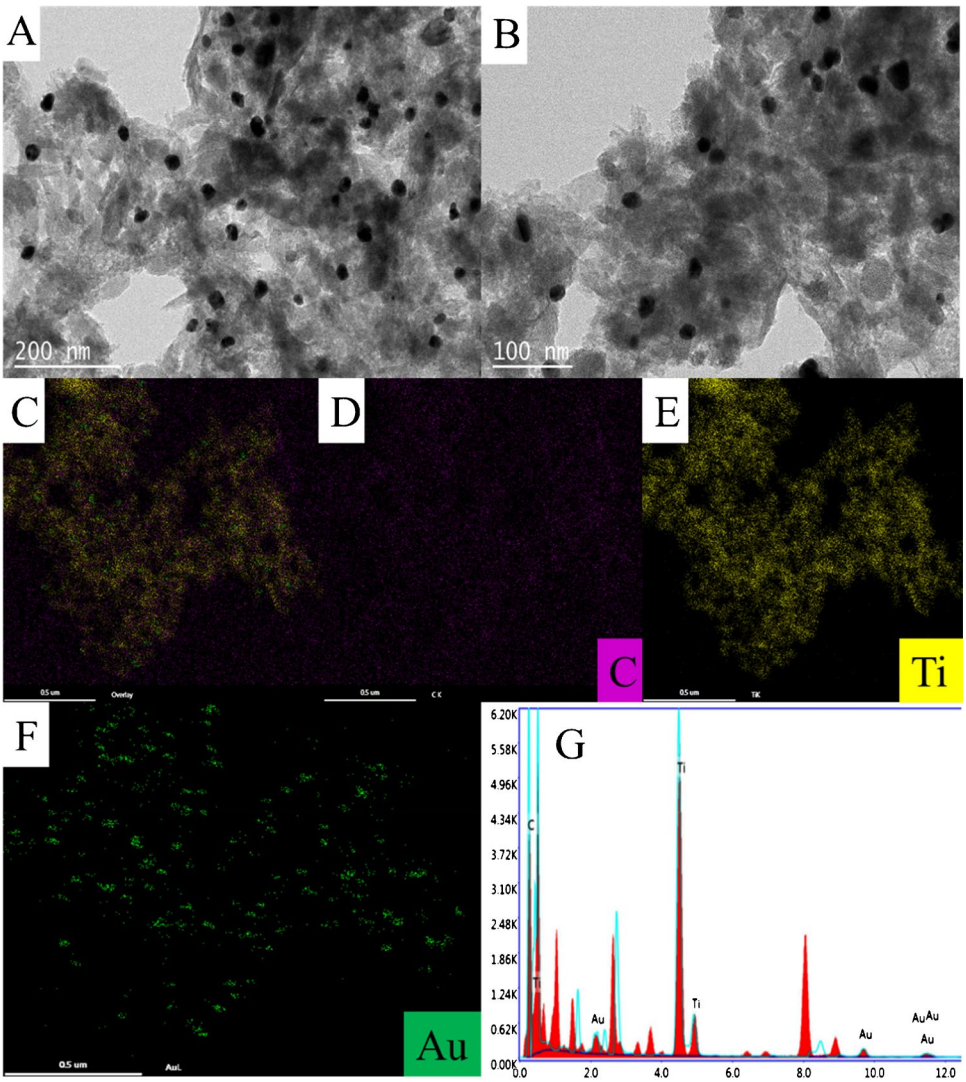

Fig. 1 TEM of MXene@Au in different sizes (**A**, **B**). MXene@Au element mapping of C, Ti, and Au (**C**, **D**, **E**, **F**). EDS images (**G**)

images (Fig. 1C, D, E, F) and EDS images (Fig. 1G) show the uniform distribution of C, Ti, and Au elements, with the content of C 33%, Ti 65%, and Au 3%, and the high proportion of Ti elements. Ti is the main form of MXene@Au. The above figures are proof that AuNPs are successfully prepared on the surface of MXene.

Characterization of AuNPs and Au@SiO_2

The newly prepared AuNPs and Au@SiO_2 were characterized with UV. As shown in Fig. 2D(a), AuNPs have a characteristic UV absorption peak at 524 nm [23], indicating that the newly prepared gold nanoparticles have good performance and uniform particle size. As shown in Fig. 2D(b), Au@SiO_2 has a characteristic UV absorption peak at 539 nm [22]. Compared with AuNPs, the absorption peak decrease significantly, and the absorption peak appear red shift. It is proved that SiO_2 shell is successfully coated on the surface of AuNPs. The peak pattern is sharp, indicating that Au@SiO_2 is well prepared. The morphological characteristics of AuNPs and Au@SiO_2 were characterized by TEM (Fig. 2A, 2B). As shown in Fig. 2A, the gold nanoparticles appear to be uniformly spherical, with uniform particle size and relatively uniform distribution. The average particle size is 27 nm (Supplementary material Fig. S1). The above results show that the synthesized gold nanoparticles have uniform color, uniform particle size, and stable electrochemiluminescence properties, which meet the experimental requirements. The synthesized Au@SiO_2 can be clearly seen in Fig. 2B, showing a high-quality core–shell structure, the gold nanoparticles are encapsulated in a silicon shell. The thickness of SiO_2 shell and the particle size of gold core were measured by TEM (Supplementary material Fig. S2). The thickness of

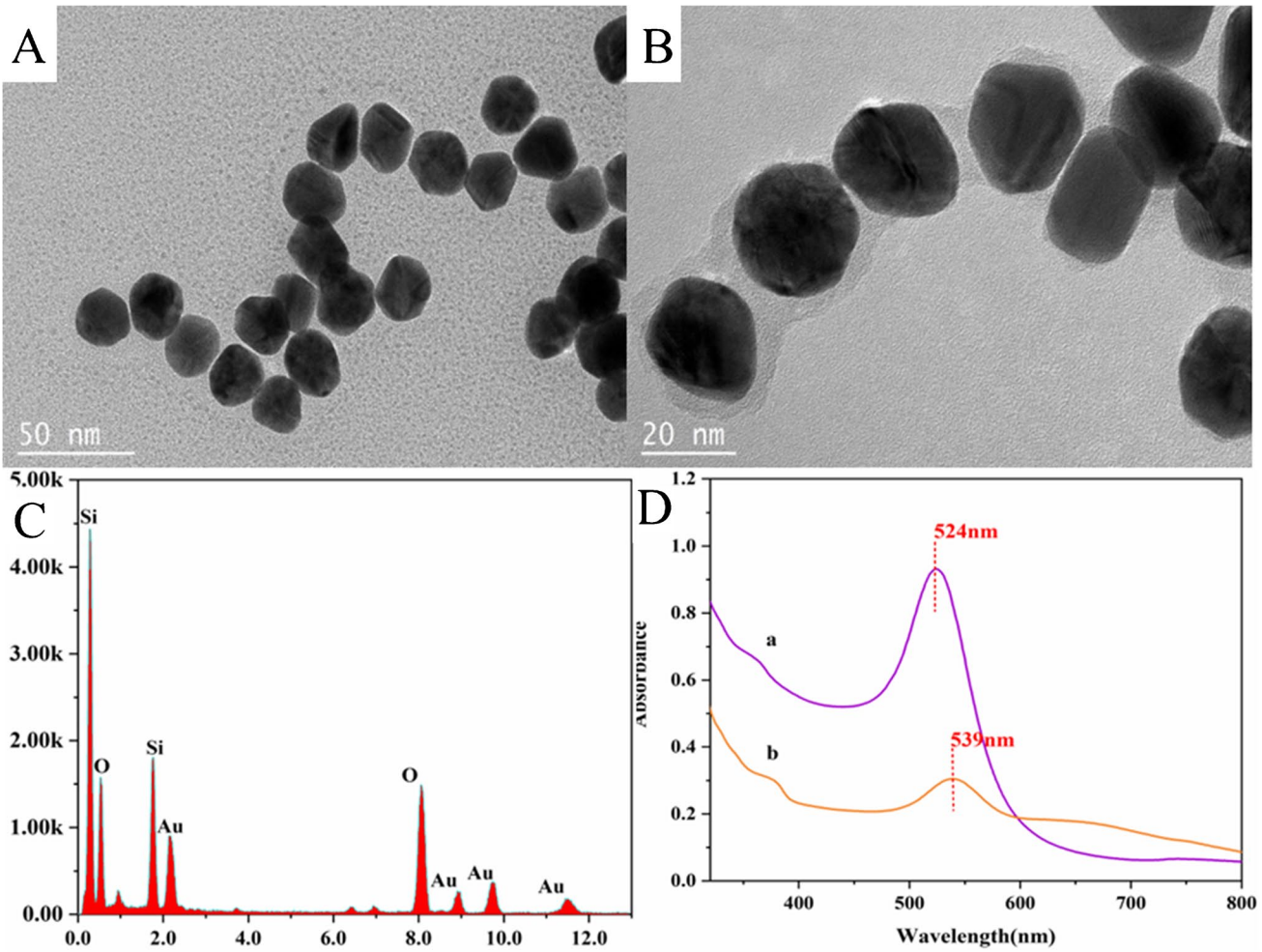

Fig. 2 TEM of AuNPs and Au@SiO_2 in different sizes (**A**, **B**). EDS images (**C**). UV absorption spectrum of AuNPs (a) and Au@SiO_2 (b) (**D**)

SiO_2 shell is 4 nm, the size of gold core is 27 nm. The core and shell structure is well dispersed and the particle size is uniform. In addition, EDS shows that all elements are evenly distributed; corresponding element mapping images (Fig. S3A, B, C, D) and EDS images (Fig. 2C) show the uniform distribution of O, Si, and Au elements, with the content of O 33.60%, Si 35.89%, and Au 30.51%. It proves that Au@SiO_2 core–shell structure is successfully prepared.

Electrochemical characterization biosensor

Through the manufacturing process of biosensor, CV characterization of electrodes in different modification stages was carried out. As shown in Fig. 3A, the electrode surface is modified MXene@Au (curve b); MXene has good conductivity, enhancing the electron transfer rate on the electrode surface; and the redox peak current is significantly higher than that of the bare electrode (curve a). After the aptamer S1 is fixed, the current response is slightly reduced (curve c) because of the aptamers blocking electron transport. With the continuous addition of Au@SiO_2 solution, the outer silicon shell reduces the conductivity of the electrode, resulting in a decrease in the peak value of the electrode (curve d). After S2 is added, complementary base pairing is conducted between aptamers, further hindering electron transmission, and the peak current of the electrode decreased (curve e). After Pb^{2+} is added (curve f), the aptamer is sheared and most of Au@SiO_2 fall off, and the peak electrode current is not significantly reduced.

The assembly process of biosensor was characterized by EIS, as shown in Fig. 3B. The electron transfer changes in electrode assembly are consistent with the CV; it shows that the sensor meet the expected effect of the experiment.

The ECL strength of nanomaterials modified electrodes are analyzed. As shown in Fig. 3C, when SiO_2 is added separately, the ECL signal of the sensor is not obvious. When $Ru(bpy)_3^{2+}$ solution is dropped on the surface of the bare electrode, it can be clearly seen that the ECL signal of the sensor is low (curve b). When AuNPs modified the

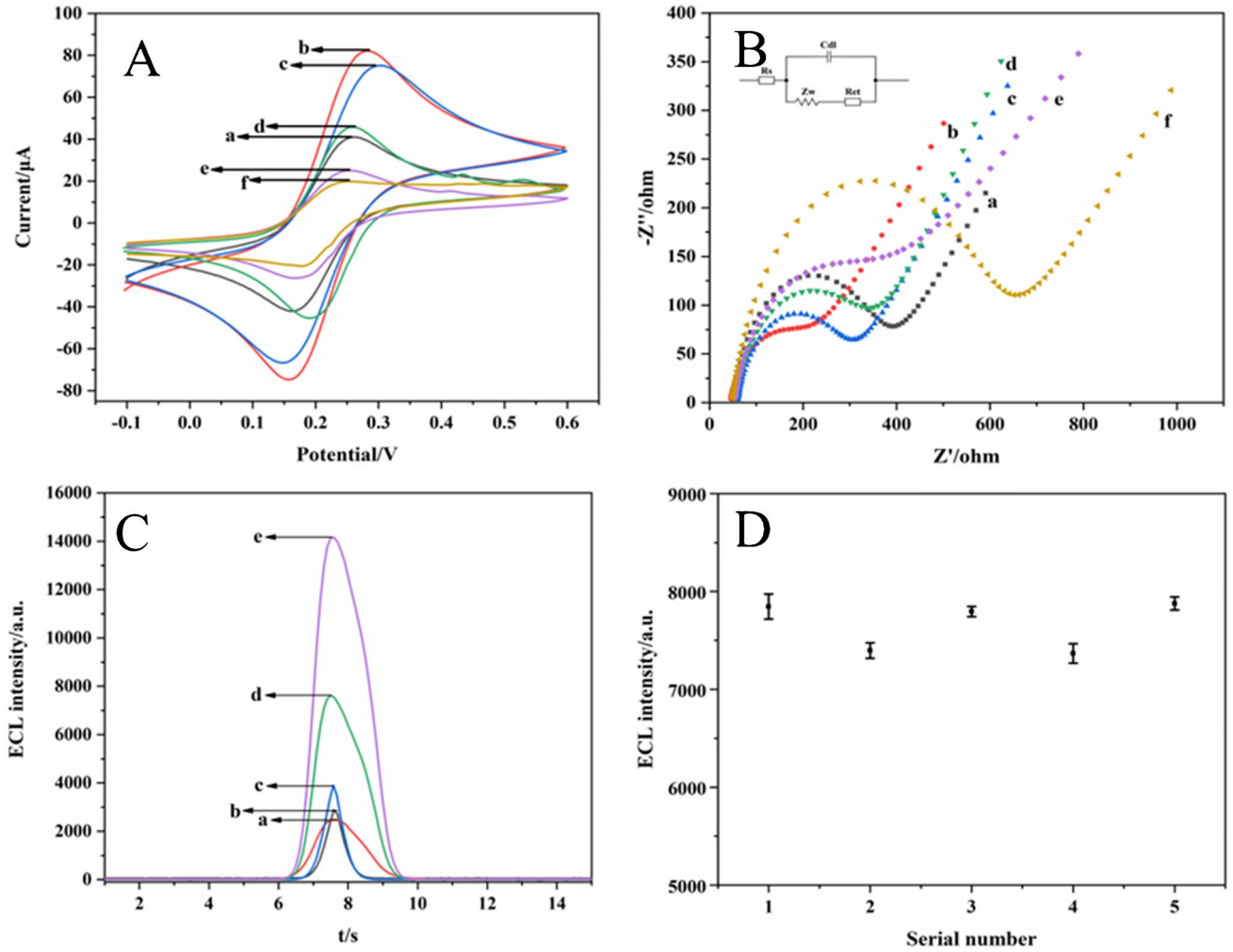

Fig. 3 **A** CV characterization diagram: (a) bare GCE; (b) Ru/Mxene@Au/GCE; (c) apt1/Ru/Mxene@Au/GCE; (d) Au@SiO_2/apt1/Ru/Mxene@Au/GCE; (e) apt2/Au@SiO_2/apt1/Ru/Mxene@Au/GCE; (f) Pb^{2+}/apt2/Au@SiO_2/apt1/Ru/Mxene@Au/GCE. **B** EIS characterization diagram: (a) bare GCE; (b) Ru/Mxene@Au/GCE; (c) apt1/Ru/Mxene@Au/GCE; (d) Au@SiO_2/apt1/Ru/Mxene@Au/GCE; (e) apt2/Au@SiO_2/apt1/Ru/Mxene@Au/GCE; (f) Pb^{2+}/apt2/Au@SiO_2/apt1/Ru/Mxene@Au/GCE. **C** ECL intensity of material: (a) SiO_2/$Ru(bpy)_3^{2+}$/GCE; (b) $Ru(bpy)_3^{2+}$/GCE; (c) AuNPs/$Ru(bpy)_3^{2+}$/GCE; (d) MXene@Au/$Ru(bpy)_3^{2+}$/GCE; (e) Au@SiO_2/$Ru(bpy)_3^{2+}$/GCE. **D** The stability of $Ru(bpy)_3^{2+}$ ECL signal on MXene@Au

electrode, it promote the luminescence signal (curve c). When MXene@Au modified the electrode, the ECL signal increases due to the excellent conductivity of MXene and π-π conjugate stacking effect (curve d). However, after Au@SiO_2 is modified on the electrode surface, because of its action of plasma resonance, the electron transfer rate is accelerated, and the ECL signal increases suddenly (curve e). The research shows that when AuNPs or SiO_2 nanomaterials exist alone, the light emission is not obvious when excited-state $Ru(bpy)_3^{2+*}$ return to its ground state $Ru(bpy)_3^{2+}$. The ECL intensity can be effectively improved after SiO_2 is coated on the surface of AuNPs. Therefore, the prepared Au@SiO_2 core–shell nanomaterials can accelerate the oxidation of TPrA and significantly enhance the ECL intensity, which confirms the feasibility of the experiment. As shown in Fig. 3D, the stability of $Ru(bpy)_3^{2+}$ ECL signal on MXene@Au is analyzed. Through the analysis and comparison of five groups of data, the ECL strength of $Ru(bpy)_3^{2+}$ is relatively stable, which proves the successful preparation of the material and ensures the sensitivity of the sensor.

The principle of Au@SiO_2 nanomaterials promote ECL intensity

The principle of Au@SiO_2 to enhance the intensity of ECL is shown in Fig. 4. $Ru(bpy)_3^{2+}$ and TPrA are typical redox luminescence systems. First of all, $Ru(bpy)_3^{2+}$ and TPrA are oxidized on the electrode surface to form $Ru(bpy)_3^{3+}$ and $TPrA^{\cdot+}$. $TPrA^{\cdot}$ is unstable and easy to lose H^+ to form $TPrA^{\cdot}$, and $TPrA^{\cdot}$ has strong reducibility to

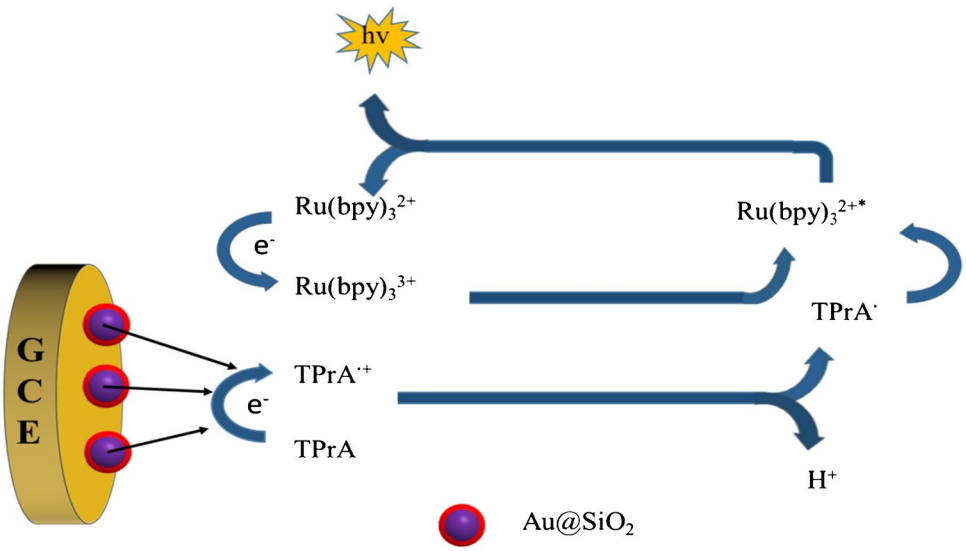

Fig. 4 Principle of $Au@SiO_2$ promoting ECL intensity of $Ru(bpy)_3^{2+}$/TPrA system

reduce $Ru(bpy)_3^{3+}$ to $Ru(bpy)_3^{2+*}$. Instable $Ru(bpy)_3^{2+*}$ release light energy returning to the ground state. The $Au@SiO_2$ plasma resonance energy transfer can improve the excitation efficiency of electromagnetic field around gold nucleus, accelerate the oxidation of TPrA, increase the light energy release of Ru $(bpy)_3^{2+*}$ returning to the ground state, and enhance the ECL intensity.

As shown in Fig. S4, EIS maps of various electrodes are described. From the EIS curves, it can be seen that the electron transfer resistance (RCT) of different electrode surfaces increase after modification. The increase of RCT is because the electron transfer rate of SiO_2 is lower than that of AuNPs. In addition, electronegative nanoparticles (such as AuNPs, SiO_2 nanoparticles, and $AuNP@SiO_2$) repel the electronegative $Fe(CN)_6^{3-/4-}$, so a higher RCT is observed. In addition, after the electrode surface is modified with AuNPs, SiO_2 coat can effectively prevent the transfer of AuNP energy, which means that more $Ru(bpy)_3^{2+}$ can react on the surface, making the ECL luminescence effect more obvious. As shown in Fig. 3C (curve e), $AuNP@SiO_2$ modified GCE is much higher than that modified by SiO_2 nanoparticles. Another possible cause may be the LSPR of AuNP. LSPR will generate a strong electromagnetic field near the surface of metal nanoparticles, which can improve the excitation rate and emission factor.

Optimization of experimental parameters

By studying the optimal experimental conditions, the aptamer concentration, culture time, and pH value of PBS substrate were optimized. The optimal aptamer concentration obtained by the electrochemiluminescence biosensor is 200 nM, the culture time is 50 min, and the pH value is 8.0. The detailed optimization data are in the supplementary material (Fig. S5).

Performance analysis of ECL biosensor

The biosensor was used to detect Pb^{2+} in water samples under optimal detection conditions. Figure 5 shows the relationship between Pb^{2+} concentration and ECL intensity. When the Pb^{2+} concentration gradually increases, the ECL signal decreases slowly (Fig. 5A). According to the limit standard of heavy metals in food formulated (CODEX STAN 193–2015) by the Codex Alimentarius Commission (CAC), the minimum limit of Pb^{2+} is 0.01 mg/kg. In the concentration range of 0.1 to 1×10^6 ng L^{-1}, the logarithm of ECL intensity and Pb^{2+} concentration shows a good linear relationship (Fig. 5B). Pb^{2+} standard curve is $I_{ECL}=8274.00–903.73lgC_{Pb}^{2+}$ ($R^2=0.998$, C_{Pb}: ng L^{-1}), and the detection limit (LOD) is 0.059 ng L^{-1} which is estimated as follows: $LOD=3\sigma/S$, where σ is the relative standard deviation of the unlabeled sample and S is the slope of the calibrated curve.

Table 1 lists and compares the relevant parameters of Pb^{2+} sensors detected by different methods in recent years, and the results show that this biosensor provides a good strategy for detecting Pb^{2+}.

Stability, reproducibility, and specificity of ECL biosensors

Figure S6A shows the stability test of the biosensor. The same four modified electrodes are used in the experiment. For the stability test of the sensor, different time periods

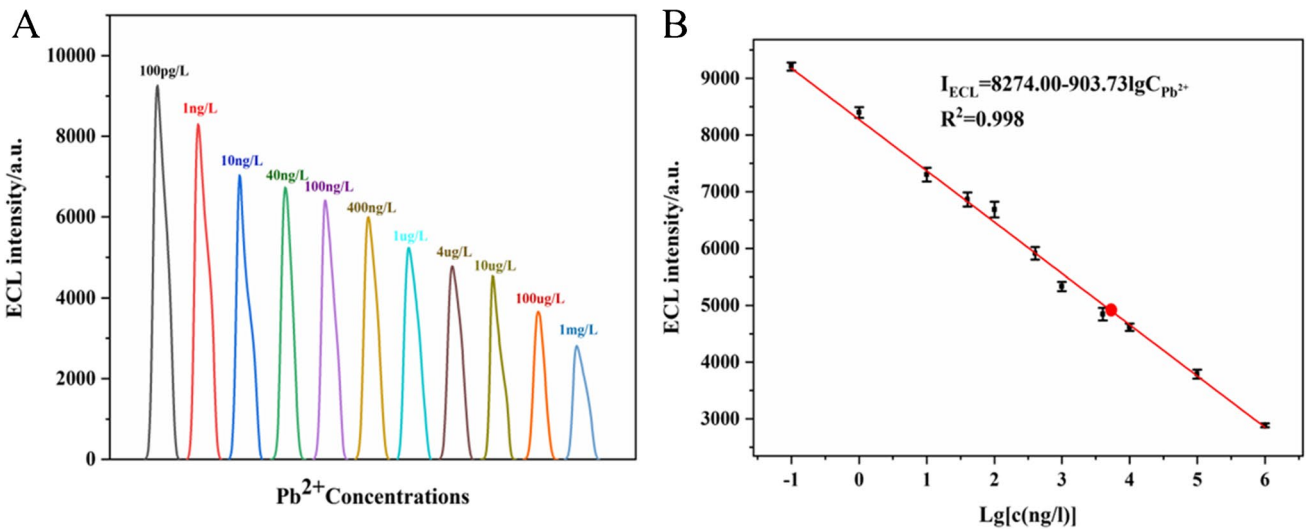

Fig. 5 ECL diagram corresponding to different Pb^{2+} concentrations (**A**); linear relationship between $Pb.^{2+}$ concentration and ECL intensity (the red dots represent blank space) (**B**)

Table 1 Determination of related parameters of Pb^{2+} by different methods

Methods	Material	Sample	Detection range (ng/L)	LOD (ng/L)	Reference
Electrochemistry	(Ag-Au) NPs	Pb^{2+}	1.0×10^{1}–1×10^{4}	3.9	[24]
	AuNPs	Pb^{2+}	1.0×10^{2}–1×10^{5}	1.0×10^{2}	[25]
	ZnO	Pb^{2+}	1.0×10^{4}–1.4×10^{5}	3.9×10^{2}	[26]
	rGO@CNT@Fe_2O_3	Pb^{2+}	4.1×10^{3}–5.4×10^{4}	2.0×10^{1}	[27]
	BFS	Pb^{2+}	1.0×10^{5}–1.7×10^{8}	1.7×10^{4}	[28]
Fluorescence	GQDs	Pb^{2+}	2.0×10^{3}–1×10^{11}	2.0×10^{4}	[29]
	NH_2-MIL-125(Ti) MOF	Pb^{2+}	0–2.3×10^{3}	1.6	[30]
ECL	Au nanocubes	Pb^{2+}	2.0×10^{1}–4.1×10^{5}	0.6	[31]
	BP nanoflakes	Pb^{2+}	0.1–1.0×10^{3}	5.6×10^{-2}	[32]
	MIL-53(Al)@CdTe-PEI	Pb^{2+}	2.0×10^{1}–2×10^{5}	7.7	[33]
	MXene@Au, Au@SiO_2	Pb^{2+}	0.1–1.0×10^{6}	5.9×10^{-2}	This work

(0 day, 5 days, 10 days, 15 days, 20 days, 25 days, and 30 days) are selected to detect the modified electrodes, and the ECL intensity of the four electrodes only decrease by 2.04% ($RSD = 1.14\%$, $n = 3$). The results show that the ECL signal of the modified electrode has no obvious change, indicating that the sensor had good stability.

Four identical modified electrodes are selected to study the reproducibility of biosensor for the detection of heavy metal Pb^{2+} with a concentration of 1000 ng L^{-1} in water samples. The results show that the RSD of the four modified electrodes is 1.02% ($n = 3$) (Fig. S6B), indicating that the biosensor has good reproducibility.

As shown in Fig. 6A and 6B, in order to test the specificity of the biosensor, nine representative metal ions are selected for study with a concentration of 5000 ng L^{-1} (Pb^{2+} concentration was 1000 ng L^{-1}). The results show that Ag^{+}, Cd^{2+}, Co^{2+}, Cu^{2+}, Fe^{3+}, Hg^{2+}, Mg^{2+}, Ni^{2+}, and Zn^{2+} have no obvious effect on the detection of Pb^{2+}, indicating that the biosensor has good specificity.

Detection of Pb^{2+} in real water samples

Laboratory tap water, Jixia lake water, and factory wastewater were selected as experimental objects. Pb^{2+} with concentrations of 10 ng L^{-1}, 100 ng L^{-1}, and 1000 ng L^{-1} were added to the three water samples, and the constructed sensors were used for testing. In order to verify the recovery test effect, the standard addition detection method was used for detection. As shown in Table 2, the recovery rate of spiked standard is between 90.00 and 125.70%, indicating that the sensor has good detection effect on Pb^{2+} in actual water samples, which proves that the strategy is true and reliable.

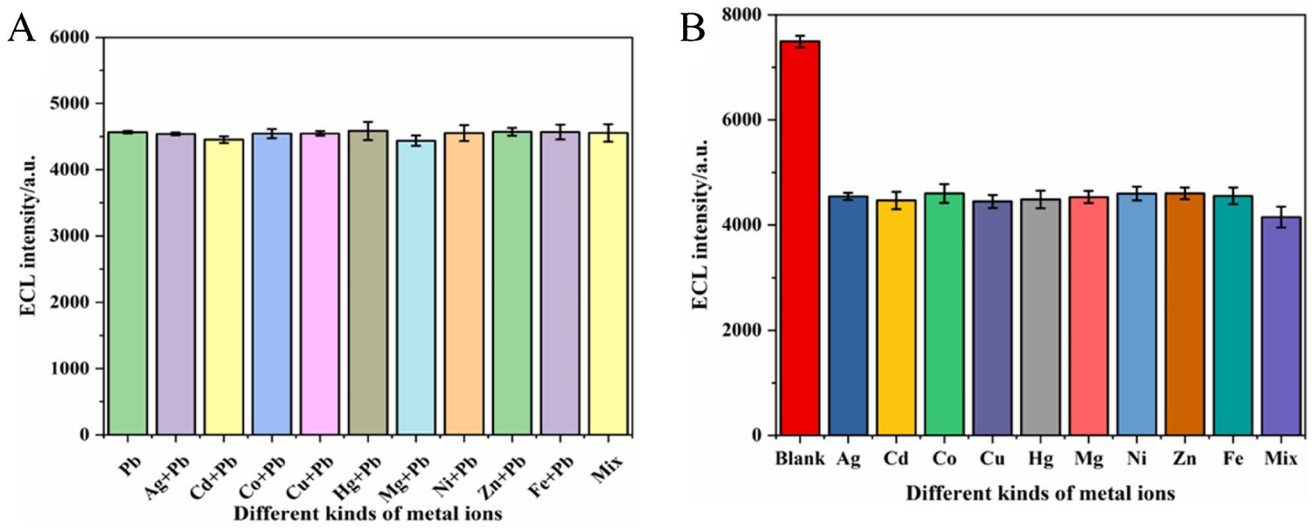

Fig. 6 ECL intensity of specificity (**A** and **B**)

Table 2 Pb^{2+} detection results of actual water sample ($n = 3$)

Target	Sample	Spiked ($ng \cdot L^{-1}$)	This method		
			Found ($ng \cdot L^{-1}$)	Recovery (%)	RSD (%)
Pb(II)	Tap water	10	10.00	90.00	0.81
		100	102.33	101.33	0.61
		1000	1258.00	125.70	0.53
	Lake water	10	10.00	90.00	0.51
		100	120.23	119.23	0.99
		1000	977.23	97.62	0.59
	Industry wastewater	10	12.30	113.00	0.52
		100	102.32	101.32	0.39
		1000	1095.72	109.47	0.67

Conclusion

In this work, the experiment of synthetic MXene@Au as the base material was used to increase the conductivity of biosensor. The $Au@SiO_2$ taking advantage of resonance energy transfer increases the excitation rate of $Ru(bpy)_3^{2+}$, speeds up the catalytic process of TPrA, and enhances the strength of ECL. Luminous effect of $Au@SiO_2$ is 5 times that of AuNP or SiO_2 nanomaterials alone. As the recognition element of Pb^{2+}, aptamer plays a role of endonuclease to realize the cascade cycle amplification and ultra-sensitive detection of Pb^{2+}. It is found that resonance energy transfer can obviously enhance the electrochemiluminescence intensity, which provides a new idea for choosing electrode material and improving the sensitivity of biosensor. At present, the water has a complex matrix, there are not only heavy metal pollution in water, but also other pollutants. For detection of one target, the ECL biosensor has some limitations. Therefore, the simultaneous detection of two or more pollutants by electrochemiluminescence biosensor will be a research hotspot.

Supplementary Information The online version contains supplementary material available at https://doi.org/10.1007/s00604-022-05429-9.

Funding This work was supported by the Natural Science Foundation of Shandong Province (ZR2018BC055) and the National Natural Science Foundation of China (No. 32161133008).

Declarations

Conflict of interest The authors declare no competing interests.

References

1. Ziaee F, Ziaee M, Taseidifar M (2021) Synthesis and application of a green surfactant for the treatment of water containing PFAS/hazardous metal ions. J Hazard Mater 407:124800
2. Mukherjee I, Singh UK, Singh RP, Anshumali D, Kumari PK, Jha P. Mehta (2020) Characterization of heavy metal pollution in an anthropogenically and geologically influenced semi-arid region of east India and assessment of ecological and human health risks. Sc Total Environ. 705:135801
3. Rahman MATMT, Paul M, Bhoumik N, Hassan M, Alam MK, Aktar Z (2020) Heavy metal pollution assessment in the groundwater of the Meghna Ghat industrial area, Bangladesh, by using water pollution indices approach. Appl Water Sci. 10:186
4. Ubando AT, Africa ADM, Maniquiz-Redillas MC, Culaba AB, Chen WH, Chang JS (2021) Microalgal biosorption of heavy metals: a comprehensive bibliometric review. J Hazard Mater 402:123431
5. Jeong H, Choi YY, Lee J, Lim J, Ra K (2020) Heavy metal pollution by road-deposited sediments and its contribution to total suspended solids in rainfall runoff from intensive industrial areas. Environ Pollut 265:115028
6. Bozorgzadeh E, Pasdaran A, Ebrahimi-Najafabadi H (2021) Determination of toxic heavy metals in fish samples using dispersive micro solid phase extraction combined with inductively coupled plasma optical emission spectroscopy. Food Chem 346:128916
7. Subramanian V, Lee S, Jena S, Jana SK, Ray D, Kim SJ, Thalappil P (2020) Enhancing the sensitivity of point-of-use electrochemical microfluidic sensors by ion concentration polarisation-a case study on arsenic. Sens Actuators B Chem 304:127340
8. Khan MS, Ameer H, Ali A, Li YY, Yang L, Ren X, Wei Q (2020) Electrochemiluminescence behaviour of silver/$ZnIn_2S_4$/reduced graphene oxide composites quenched by Au@SiO_2 nanoparticles for ultrasensitive insulin detection. Biosens Bioelectron 162:112235
9. Praoboon N, Siriket S, Taokaenchan N, Kuimalee S, Phaisaqnsuthichol S, Pookmanee P, Satienperakul S (2022) Paper-based electrochemiluminescence device for the rapid estimation of trimethylamine in fish via the quenching effect of thioglycolic acid-capped cadmium selenide quantum dots. Food Chem 366:130590
10. D'Alton L, Nguyen P, Carrara S, Hogan CF (2021) Intense near-infrared electrochemiluminescence facilitated by energy transfer in bimetallic Ir-Ru metallopolymers. Electrochim Acta 379:138117
11. AL-maskri AAA, Ye JW, Talap J, Hu HH, Sun LL, Yu LS, Cai S, Zeng S (2020) Reverse transcription-based loop-mediated isothermal amplification strategy for real-time miRNA detection with phosphorothioated probes, Anal Chim Acta. 1126 1-6
12. Jiang CM, Li XJ, Yao Y, Lan LY, Shao YZ, Zhao FN, Ying YB, Ping JF (2020) A multifunctional and highly flexible triboelectric nanogenerator based on MXene-enabled porous film integrated with laser-induced graphene electrode. Nano Energy 66:104121
13. Shao YZ, Yao Y, Jiang CM, Zhao FN, Liu XX, Ying YB, Ping JF (2019) Two-dimensional MXene nanosheets (types $Ti_3C_2T_x$ and Ti_2CT_x) as new ion-to-electron transducers in solid-contact calcium ion-selective electrodes. Microchim Acta 186:750
14. Downs AM, Gerson J, Hossain MN, Ploense K, Pham M, Kraatz HB, Kippin T, Plaxco KW (2021) Nanoporous gold for the miniaturization of in vivo electrochemical aptamer-based sensors. ACS Sens 6:2299–2306
15. Idili A, Parolo C, Alvarez-Diduk R, Merkoci A (2021) Rapid and efficient detection of the SARS-CoV-2 spike protein using an electrochemical aptamer-based sensor. ACS Sens 6:3093–3101
16. Hedarian SMT, Sani AT, Danesh NM, Ramezani M, Alibolandi M, Gerayelou G, Abnous K, Taghdisi SM (2021) A novel electrochemical approach for the ultrasensitive detection of fluoroquinolones based on a double-labelled aptamer to surpass complementary strands of aptamer lying flatSens. Actuators B Chem 334:129632
17. Sahin S, Caglayan MO, Ustundag Z (2020) A review on nanostructure-based mercury (II) detection and monitoring focusing on aptamer and oligonucleotide biosensors. Talanta 220:121437
18. Wang WR, Xu YC, Cheng N, Xie YX, Huang KL, Xu WT (2020) Dual-recognition aptazyme-driven DNA nanomachine for two-in-one electrochemical detection of pesticides and heavy metal ions. Sens Actuators B Chem 321:128598
19. Yu ZZ, Jiang L, Liu RY, Zhao WD, Yang ZH, Zhang JY, Jin SZ (2021) Versatile self-assembled MXene-Au nanocomposites for SERS detection of bacteria, antibacterial and photothermal sterilization. Chem Eng J 426:131914
20. Zhao FN, Yao Y, Jiang CM, Shao YZ, Barcelo D, Ying YB, Ping JF (2019) Self-reduction bimetallic nanoparticles on ultrathin MXene nanosheets as functional platform for pesticide sensing. Journal of Haardous Materials 384:121358–121358
21. Yao Y, Lan LY, Liu XX, Ying YB, Ping JF (2019) Spontaneous growth and regulation of noble metal nanoparticles on flexible biomimetic MXene paper for bioelectronics. Biosens Bioelectron 148:111799
22. Wang DF, Guo LH, Huang R, Qiu B, Lin ZY, Chen GN (2015) Surface enhanced electrochemiluminescence of $Ru(bpy)_3^{2+}$. Sci Rep 5:7954
23. Huang JC, Xiang YD, Li JS, Kong QQ, Zhai HG, Xu R, Yang FZ, Sun X, Guo YM (2021) A novel electrochemiluminescence aptasensor based on copper-gold 5 bimetallic nanoparticles and its applications. Biosens Bioelectron 194:113601
24. Yadav, Y., Berlina, A.N., Zherdev, A.V., Gaur, M.S., Dzantiev, Rapid and selective electrochemical detection of Pb^{2+} ions using aptamer-conjugated alloy nanoparticles, SNAS 2077 (2020).
25. Abu-Ali H, Nabok A, Smith TJ (2019) Development of novel and highly specific ssDNA-aptamer-based electrochemical biosensor for rapid detection of mercury (II) and lead (II) ions in water. Chemosensors 27:2–14
26. Oliveira VHB, Rechotnek F, Silva E, Marques VDS (2020) A sensitive electrochemical sensor for Pb^{2+} ions based on ZnO nanofibers functionalized by L-cysteine. J Mol Liq 309:113041
27. Fall B, Diaw AKD, Fall M, Sall ML (2021) Synthesis of highly sensitive rGO@CNT@Fe_2O_3/polypyrrole nanocomposite for the electrochemical detection of Pb^{2+}. Mater Today Commun 334:102005
28. Mourya A, Sinha SK, Mazumdar B (2019) Glassy carbon electrode modified with blast furnace slag for electrochemical investigation of Cu^{2+} and Pb^{2+} metal ions. Microchemical J 149:113041
29. Raj SK, Yadav V, Bhadu GR, Patidar R, Kumar M, Kulshrestha V (2021) Synthesis of highly fluorescent and water soluble graphene quantum dots for detection of heavy metal ions in aqueous media. Environ Sci Pollut Res 28:46336–46342
30. Vekateswarlu S, Reddy AS, Panda A, Sarkar D, Son YH, Yoon MY (2020) Reversible fluorescence switching of metal-organic framework nanoparticles for use as security ink and detection of Pb^{2+} ions in aqueous media. ACS Appl Nano Mater 4:3684–3692
31. Zhang Y, Xu JM, Zhou S, Zhu L, Lv X, Zhang J, Zhang LN, Zhu PW, Yu JH (2020) DNAzyme-triggered visual and ratiometric

electrochemiluminescence dual-readout assay for Pb(II) based on an assembled paper device. Anal Chem 92:3874–3881
32. Wang YH, Shi HH, Zhang LN, Ge SG, Xu ML, Wang X, Yu JH (2021) Two-dimensional black phosphorus nanoflakes: a co-reactant-free electrochemiluminescence luminophors for selective Pb^{2+} detection based on resonance energy transfer. J Hazard Mater 403:123601
33. Feng DF, Li PH, Tan XC, Wu YY, Wei FC, Du FK, Ai CH, Luo YN, Chen QY, Han HY (2020) Electrochemiluminescence aptasensor for multiple determination of Hg^{2+} and Pb^{2+} ions by using the MIL-53(Al)@CdTe-PEI modified electrode. Anal Chim Acta 1100:232–239